LETTERS

Persistence of full glacial conditions in the central Pacific until 15,000 years ago

P.-H. Blard[1,2]†, J. Lavé[3]†, R. Pik[2], P. Wagnon[4] & D. Bourlès[1]

The magnitude of atmospheric cooling during the Last Glacial Maximum and the timing of the transition into the current interglacial period remain poorly constrained in tropical regions, partly because of a lack of suitable climate records[1]. Glacial moraines provide a method of reconstructing past temperatures, but they are relatively rare in the tropics. Here we present a reconstruction of atmospheric temperatures in the central Pacific during the last deglaciation on the basis of cosmogenic ^{3}He ages of moraines and numerical modelling of the ice cap on Mauna Kea volcano, Hawaii—the only highland in the central Pacific on which moraines that formed during the last glacial period are preserved[2]. Our reconstruction indicates that the Last Glacial Maximum occurred between 19,000 and 16,000 years ago in this region and that temperatures at high elevations were about 7 °C lower than today during this interval. Glacial retreat began about 16,000 years ago, but temperatures were still about 6.5 °C lower than today until 15,000 years ago. When combined with estimates of sea surface temperatures in the central Pacific Ocean[3], our reconstruction indicates that the lapse rate during the Last Glacial Maximum was higher than at present, which is consistent with the proposal that the atmosphere was drier at that time[1,4]. Furthermore, the persistence of full glacial conditions until 15,000 years ago is consistent with the relatively late and abrupt transition to warmer temperatures in Greenland[5], indicating that there may have been an atmospheric teleconnection between the central Pacific and North Atlantic regions during the last deglaciation.

There is an important need for precise ice-retreat chronology in areas where past glaciers are the sole indicators of palaeoclimate. Mauna Kea volcano (elevation 4,206 m) is the only highland area of the central Pacific (Hawaii, 19° N) where moraines of the last glaciation have been preserved[2] (Fig. 1). Fortunately, many of the glacial deposits on Mauna Kea are not covered by volcanic material and have been exposed continuously since their formation. The emplacement of these moraines can therefore be dated by using cosmic-ray exposure methods. This late Pleistocene glacial footprint is represented by a ~10-km diameter cap of moraines draping the upper slopes of the volcano. These deposits extend downslope to a mean elevation of 3,400–3,500 m, with local outlet digitations reaching altitudes as low as 3,200 m in places such as the Pohakuloa gulch (Fig. 1c). The age of these glacial deposits has been

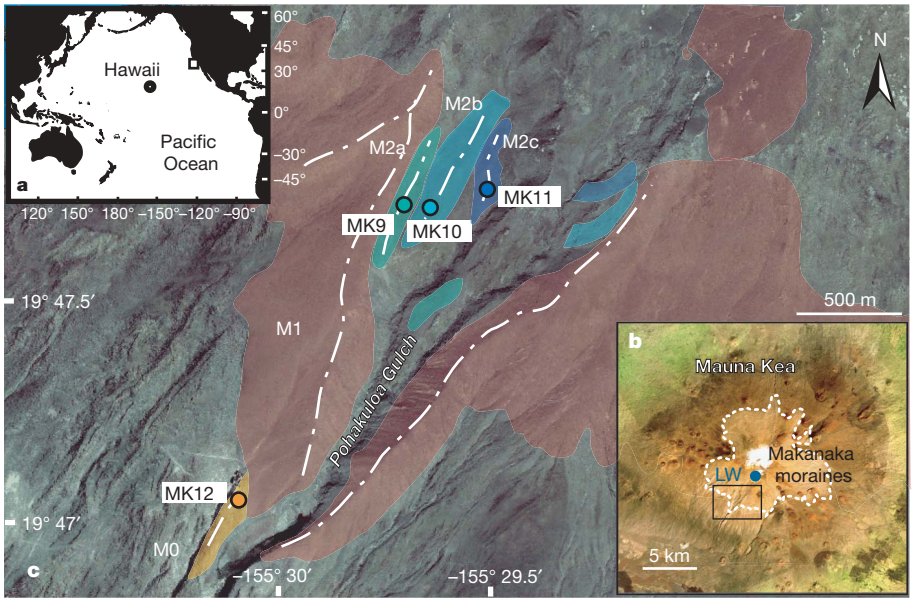

Figure 1 | Map of the sampled glacial deposits (Mauna Kea, Hawaii, central Pacific). a, Location of the Hawaiian Islands in the Pacific Ocean. The square shows the location of marine core MD02-2503, Santa Barbara Basin[27]. **b**, Location of the Pohakuloa gulch (SPOT image). LW, Lake Waiau. **c**, Map of moraines extents (M0 in orange, M1 in red, M2a, M2b and M2c in blue) and locations of the sampled boulders.

[1]Centre Européen de Recherche et d'Enseignement des Géosciences de l'Environnement, CNRS – Aix Marseille Université, 13545 Aix en Provence, France. [2]Centre de Recherches Pétrographiques et Géochimiques, CNRS, 54501 Vandoeuvre-lès-Nancy, France. [3]Laboratoire de Géodynamique des Chaînes Alpines, CNRS – Université Joseph Fourier, 38400 Grenoble, France. [4]Institut de Recherche Pour le Développement, Great Ice, Laboratoire de Glaciologie et Géophysique de l'Environnement, 38402 Grenoble, France. †Present addresses: Geological and Planetary Science Division, California Institute of Technology, MC 100-23, 1200 E. California Boulevard, Pasadena, California 91125, USA (P.-H.B.); Centre de Recherches Pétrographiques et Géochimiques, CNRS, 54501 Vandoeuvre-lès-Nancy, France (J.L.).

roughly constrained between 31 ± 9 and 18 ± 10 kyr BP (errors are 1σ) by K–Ar dating of interbedded lavas[6]. Two cosmogenic ^{36}Cl ($^{36}Cl_c$) data on the main moraine M1 yielded ages of 18.9 ± 0.8 and 20.3 ± 2.3 kyr (ref. 7). The errors accompanying these ages, however, are analytical only and should include the ~30% uncertainties[8] in the production rate of $^{36}Cl_c$. More precise ages can be determined by using cosmogenic ^{3}He (^3He_c) because its production rate is known with better precision (1σ < 10%). However, measuring ^3He_c exposure ages requires the presence of the mineral olivine or pyroxene[9]. The only glacial deposits filling this petrological criterion were encountered within the Pohakuloa gulch (Fig. 1c). The shoulders dominating this talweg are the massive lateral moraine M1, whose frontal termination extends downslope to ~3,200 m, where it locally overlays frontal deposit M0 (Fig. 1c). M0 is interpreted as a subdued frontal moraine deposited in front of the Pohakuloa glacial tongue during its initial advance of the Last Glacial Maximum (LGM). M0 thus pre-dates the building of the main moraine M1. Three boulders ~1 m high (MK12A, MK12B and MK12C) have been sampled at ~3,200 m on M0 (Fig. 1c and Supplementary Table 1) to determine a maximum age for M1.

The retreat after the maximal ice extension is marked by three small recessional moraine deposits, M2a, M2b and M2c, extending from ~3,500 to 3,700 m within the inner part of the Pohakuloa gulch (Fig. 1c). To document the timing of glacial retreat, seven cobbles and boulders were sampled on M2a (MK9A, MK9B, MK9D and MK9F) and M2b (MK10A, MK10B and MK10C) at ~3,600 m, as well as the top of a large striated erratic block (MK11) in the M2c unit (Fig. 1c and Supplementary Table 1).

Measurement of cosmogenic ^{3}He concentrations is described in Methods. ^3He_c data were converted into exposure ages by using the ^3He_c production rate calibrated in Hawaii[10]. A sampling test performed on M2 led us to exclude boulders less than 80 cm in height, which improves the reliability of these cosmogenic ages (Supplementary Fig. 1).

The three boulders ~1 m high (MK12A, MK12B and MK12C) sampled in M0 have concordant ages of 17.2 ± 1.7, 19.1 ± 1.9 and 18.6 ± 1.9 kyr, respectively (Supplementary Table 1). The consistency of these ages suggests that post-depositional processes did not significantly affect the exposure history of the boulders. These data thus indicate a maximum age of ~19 kyr for the local LGM (LLGM) (Fig. 2a).

The largest boulders (more than 80 cm) from the M2 moraine yield ages ranging from 14.5 ± 1.5 to 15.7 ± 1.6 kyr. The clustering of these ages, as well as the small size of the M2 recessional moraines, suggest a short duration of the ~3,600-m stillstand at ~15.5 kyr BP. This interpretation is consistent with a $^{36}Cl_c$ exposure age of 14.7 ± 4.4 kyr from a boulder located above the M2 moraine[7]. The ^3He_c dates of M2 are also nearly synchronous with the calibrated[11] ^{14}C age of 14.7 ± 0.7 kyr from Lake Waiau[12] (3,962 m) that postdates the Mauna Kea ice cap.

We thus propose the following glacial chronology (Fig. 2a): first, initiation of the terminal moraine M0 deposition at 3,200 m by ~19 kyr BP, synchronous with or after the initial glacial advance; second, a major stillstand between 19 and 16 kyr BP, leading to the construction of the main moraine M1; third, a recessional phase at ~16 kyr BP with an episodic and short stillstand at ~15.5 kyr BP marked by the recessional moraines M2 at ~3,600 m; and fourth, a marked acceleration of retreat, leaving Mauna Kea almost completely free of ice after ~15 kyr BP. This chronology is consistent, within uncertainties, with the glacial records in the nearest glaciers of the Rocky Mountains (reviewed in ref. 13) and Mexico[14]. Dating of moraines in the tropical Andes[15] indicates an earlier local LGM there, suggesting different behaviour in the Southern Hemisphere.

To determine the high-altitude palaeoclimatic conditions in Hawaii since 19 kyr BP, the Mauna Kea ice cap has been reconstructed by using a numerical ice flux model[16] that combines both a mass-balance law and the influence of the local topography on glacier geometry (see legend to Fig. 3a). An input mass-balance curve (Fig. 3b) is calculated from a positive-degree-day (PDD) model[17] that includes temperature, precipitation, albedo and direct solar radiation (see Methods). Current temperatures are characterized by a seasonal amplitude of ~4 °C (Supplementary Fig. 3) and by a lapse rate of 5.4 ± 0.1 °C km^{-1} (Supplementary Fig. 4). The total annual precipitation decreases exponentially with elevation to a minimum of ~260 mm yr^{-1} above 4,000 m (Supplementary Fig. 5).

The presence of a glacier at 3,200 m in the Pohakuloa gulch requires lowering the equilibrium line altitude (ELA) to ~3,780 m during the LLGM (Fig. 3b). This shift is compatible with a former estimate based on the accumulation-area ratio method[18]. Assuming invariant precipitation in the PDD model, the depression in ELA requires a mean annual decrease in temperature of ~7 °C at 4,200 m. This estimate includes a correction of 1 °C, which takes into account the combined effects of subsidence and LLGM sea level lowering[19].

The sensitivity of the ELA to snowfall amount has been assessed by calculating all the (temperature, precipitation) solutions able to reproduce the decrease in ELA during the LLGM (Fig. 3c). This test shows that, in Hawaii, the ELA is more sensitive to air temperature

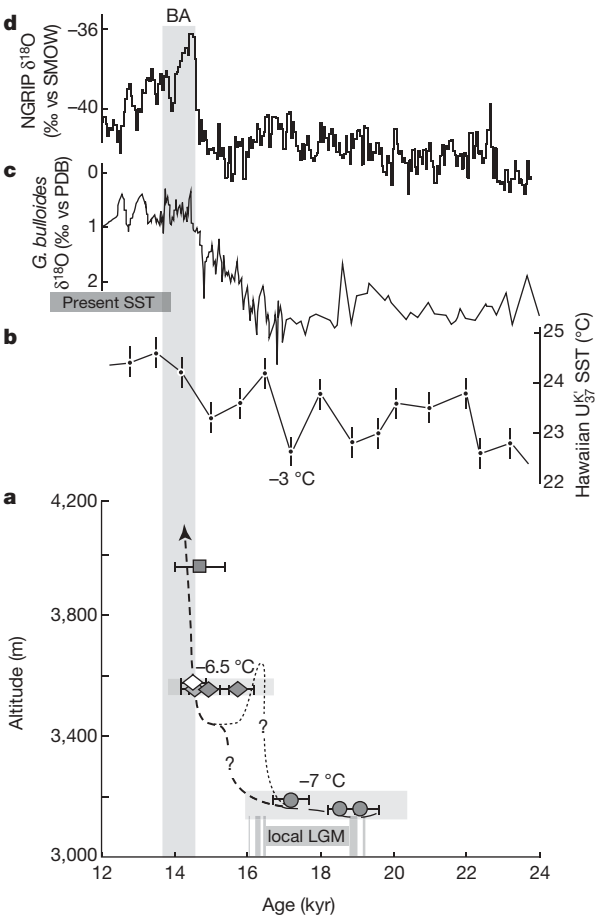

Figure 2 | Comparison of the Mauna Kea glacial chronology with other palaeoclimate proxies since 24 kyr BP. **a**, Glacial retreat chronology of the Pohakuloa gulch established by ^3He_c and ^{14}C dating[12] of moraines. Cosmogenic ages are plotted with their respective 1σ analytical uncertainties. For comparison with other absolute records, grey boxes include the 10% total uncertainty attached to production rates and scaling. Cooling values associated with each glacier position are computed for the corresponding ELA and assume invariant precipitations (Fig. 3). Grey square, ^{14}C age (ref. 12); diamonds, recessional moraines (light grey, M2a; dark grey, M2b; white, M2c); grey circles, terminal moraine M0; dashed lines, glacier front position. **b**, Hawaiian SST (PC17 core, 21° N, 158° W) from alkenone unsaturation index $U^{K'}_{37}$ (ref. 3). Error bars are shown as 1σ. **c**, δ^{18}O in *Globigerina bulloides* (SST proxy), Santa Barbara Basin (MD02-2503 core, 34° N, 120° W)[27]. **d**, $\delta^{18}O_{ice}$ (air temperature proxy) from the North Greenland Ice Core Project (NGRIP), Greenland (75° N, 42° W)[5]. BA = Bølling-Allerød.

than to precipitation variations. If, for example, precipitation is increased fivefold, a decrease in temperature of ~4.5 °C is still required to reproduce the LLGM snowline. Precipitation was probably lower during the LLGM because pollen records at 500 m elevation in Oahu Island (Hawaii) suggest that rainfall was 50–100% of present levels[20]. Thus, although some degree of decoupling may occur between low-altitude and high-altitude precipitation[21], our estimate of ~7 °C cooling at high altitudes could be considered to be a minimum value (Fig. 3c).

The accuracy of our estimate could be challenged on several counts. First, PDD models have been calibrated at high latitude and are not perfectly suited to describe outer-tropical glaciers in which daily cycles of melting are more sensitive to radiative budget than sensible heat flux[22]. However, melt data from glaciers in the tropical Andes[23] indicate that ablation is well correlated with annual variations in temperature. Moreover, the model used here was calibrated by using mass balance data from a well-documented tropical glacier (Zongo, 16° S) and includes the forcing of solar radiation and the influence of albedo (see Methods and Supplementary Information). Second, our model does not directly include effects of wind, cloudiness and air humidity, which are important in determining the mass balance of tropical glaciers and may therefore represent an important source of uncertainty. However, as reported[24], these effects can be integrated into the PDD model by varying the values of melting parameters. Thus, assessing the sensitivity of the model to extreme melting parameters (0.7-fold to 1.3-fold is the reported range for tropical glaciers[24]) provides an evaluation of the uncertainty arising from these atmospheric variables (±0.5 °C). Third, another source of uncertainty lies in the glacier dynamics model[16]. Sensitivity tests show that this imprecision is ±0.7 °C, which leads to a total uncertainty of ±0.9 °C for the model (see Supplementary Information). Last, if an extreme range in precipitation is considered (from half to double the present value[20,25]), these overall uncertainties imply that the LLGM cooling ranges between 8.3 and 5.4 °C (Fig. 3c).

This decrease in temperature is larger than the ~3.5 °C LGM cooling determined in ref. 21 at Mauna Kea. This 3.5 °C cooling was computed on the assumption that LGM precipitation (~1,600 mm yr^{-1}) were significantly above the present value of ~300 mm yr^{-1} at 3,800 m (ref. 21). With such a high snowfall, our model would yield a cooling of 4.4 ± 0.9 °C. The use of alternative precipitation may therefore partly account for the difference between both results. This previous estimate[21] also relies on a PDD model, and part of the discrepancy may also be due to the use of different melting parameters.

Coeval high-altitude ΔT of ~7 °C and local sea surface temperature (SST) cooling of ~3 °C during the LLGM[3] requires a steeper vertical gradient of surface temperature (~6.4 ± 0.2 °C km^{-1}, in contrast with the present value of 5.4 ± 0.1 °C km^{-1}). This result is qualitatively in agreement both with pollinic reconstructions[1,20] and with atmospheric general circulation models[4], indicating steeper lapse rates during the LLGM as a result of a drier tropical atmosphere. However, it should be noted that the glaciation of the Hawaiian summits possibly created a local feedback that might explain much of the high-atmosphere cooling of the area. This did not necessarily induce steeper free-air lapse rates in the whole Pacific Ocean.

If a constant lapse rate between 19 and 15 kyr BP is assumed, the glacial response shows variations in time and in temperature that are similar to those of the local Hawaiian SST[3,26] (Fig. 2a and b). Indeed, the ~0.7 °C sea surface warming between 17 and 15 kyr BP is similar to the ~0.5 °C increase necessary to trigger the increase in ELA from 3,780 to 3,880 m. Similarly, under invariant precipitation, the subsequent SST increase of 1.5 °C is sufficient to induce summit deglaciation after 15 kyr BP. Ice cap disappearance as a result of warming (rather than a decrease in precipitation) is also supported by pollinic reconstructions[20] showing that low-altitude precipitations

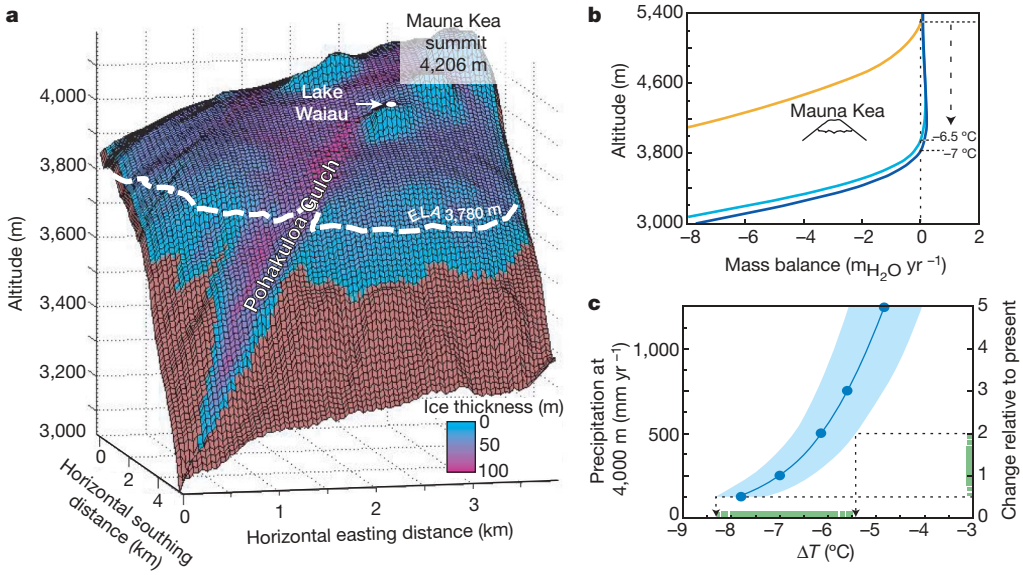

Figure 3 | Modelling of the Mauna Kea ice cap since the local Last Glacial Maximum, and palaeoclimatic reconstruction. a, Modelling of the maximal glacier extension in the Pohakuloa gulch (~3,200 m during the LLGM, 19–16 kyr BP) using the ice-flux model of ref. 16. Inputs are the 50-m-resolution digital elevation model of the Mauna Kea summit southwest area and the modelled elevation-dependent mass balance. Iterations on palaeoclimatic conditions were run until the modelled ice cap fitted the observed moraine extension. The best fit was obtained with an ELA 3,780 m high. **b**, Plot of present-day (orange), LLGM (16–19 kyr BP; dark blue) and 15 kyr BP (light blue) mass balance (MB) against elevation. MB calculations are described in Methods. The present-day Hawaiian MB curve is characterized by an ELA ~5,300 m high. The MB curve used to reproduce the LLGM extension (16–19 kyr BP) requires an ELA depression to ~3,780 m. The associated cooling is ~7 °C, under invariant precipitation. The MB corresponding to the 15 kyr BP extension yields an ELA at 3,880 m and a respective cooling of ~6.5 °C. **c**, Palaeoclimatic conditions able to reproduce the glacier extent during the local LGM (between 19 and 16 kyr BP). This plot of the change in temperature (ΔT) above 3,000 m against the change in precipitation at 4,000 m provides a direct test of the sensitivity of cooling to variations in precipitation. These climatic reconstructions are corrected for subsidence and change in sea level[19]. The dark blue line is calculated by using the model parameters calibrated from the Zongo glacier data (see Methods and Supplementary Information), the blue shading shows the total uncertainty of the model (see Supplementary Information) and the green box shows the conservative temperature interval on the assumption of a precipitation range during the LLGM of between half and double the present value[20,25].

did not decline, but actually increased by ~50% after 16 kyr BP. Even though uncertainties in timing preclude a definitive demonstration, this temperature coupling could indicate a local SST forcing of the snowline[4]. The second nearest marine core, from Santa Barbara Basin[27], provides time variations of $\delta^{18}O$ in *Globigerina bulloides* (SST proxy) showing a similar pattern (Fig. 2c). This eastern Pacific area began to warm at ~16.5 kyr BP, concurrently with the end of the Mauna Kea LLGM. Final ocean warming, after a slight cooling episode at ~15 kyr BP, was also nearly synchronous, within uncertainties, with the Hawaiian glacial retreat.

Finally, the proposed climate modelling requires the persistence of a 6.5 ± 0.9 °C cooler atmosphere until 15 kyr BP (Fig. 3b). This suggests a delayed warming of the central Pacific, whereas the southern Pacific[28] and Antarctic[29] had warmed continuously since 18 kyr BP. This late warming is concomitant with the Bølling–Allerød event and is therefore consistent with the Greenland pattern[5] (Fig. 2d). Thus, even if partly controlled by changes in SST, Hawaiian ELA fluctuations could also have been driven by an atmospheric teleconnection between the central Pacific and the northern Atlantic. Such atmosphere forcing is also supported by modelling experiments testing the sensitivity of the response of the northern Pacific to changes in the North Atlantic[30].

METHODS SUMMARY

Cosmogenic ^{3}He measurements were performed at the Centre de Recherches Pétrographiques et Géochimiques (Nancy) noble gases laboratory in accordance with the analytical procedure described previously[10]. Three samples of pure 0.5–1-mm phenocrysts were first slightly crushed *in vacuo* for evaluation of the $^3He/^4He$ magmatic ratio. To prevent any underestimate of the matrix-sited cosmogenic ^{3}He (ref. 10), the finest fraction (less than 0.15 mm) was removed before the subsequent *in vacuo* melting step. Because the contribution of magmatic helium is very low for these phenocrysts, some samples (the 0.5–1-mm fraction) were directly melted without preliminary crushing.

^3He_c concentrations (Supplementary Table 1) were calculated by assuming, first, that all ^{4}He extracted by melting was magmatic and second, that the magmatic $^3He/^4He$ ratio was 8 ± 1 Ra (where $Ra = 1.384 \times 10^{-6}$ is the atmospheric $^3He/^4He$ ratio). Post-eruptive addition of radiogenic $^4He^*$ is negligible (less than 5×10^{-15} mol g^{-1}) as a result of the low U and Th concentrations (~0.3 and 0.8 p.p.m., respectively) of these ~100-kyr-old basalts[6]. Measured ^3He_c concentrations range from 8.0×10^6 to 15.5×10^6 atoms g^{-1} and have very low analytical uncertainties ($1\sigma \approx 3\%$). Such precision was possible because the analysed phenocrysts are particularly poor in magmatic helium ($^4He < 5 \times 10^{-14}$ mol g^{-1}), and thus the correction for primordial ^{3}He does not exceed 3%. ^3He_c concentrations were converted into exposure ages by using a sea-level high-latitude production rate of 128 ± 5 atoms g^{-1} yr^{-1} (ref. 10). Geometric and time corrections of ^3He_c production rates were performed in accordance with the procedure described in Methods.

The Hawaiian palaeoclimate was determined by reconstructing past glacial extents with the use of a numerical model (Fig. 3). For this purpose, an ice-flow cellular automaton[16] was implemented with an ice mass-balance model based on a PDD approach. This PDD model includes the past variations of solar radiations[17] and the influence of albedo. The snow-rain threshold is +1 °C.

Full Methods and any associated references are available in the online version of the paper at www.nature.com/nature.

Received 22 August 2006; accepted 1 August 2007.

1. Farrera, I. *et al.* Tropical climates at the Last Glacial Maximum: a new synthesis of terrestrial palaeoclimate data. I. Vegetation, lake levels and geochemistry. *Clim. Dyn.* **15,** 823–856 (1999).
2. Porter, S. C. Hawaiian glacial ages. *Quat. Res.* **12,** 161–187 (1979).
3. Lee, K. E., Slowey, N. C. & Herbert, T. D. Glacial sea surface temperatures in the subtropical North Pacific: A comparison of U-K_{37}', $\delta^{18}O$, and foraminiferal assemblage temperature estimates. *Paleoceanography* **16,** 268–279 (2001).
4. Kageyama, M., Harrison, S. P. & Abe-Ouchi, A. The depression of tropical snowlines at the last glacial maximum: What can we learn from climate model experiments? *Quaternary Int.* **138,** 202–219 (2005).
5. Andersen, K. K. *et al.* High-resolution record of Northern Hemisphere climate extending into the last interglacial period. *Nature* **431,** 147–151 (2004).
6. Wolfe, E. W., Wise, W. S. & Dalrymple, G. B. The geology and petrology of Mauna Kea volcano, Hawaii—a study of postshield volcanism. *Prof. Pap. US Geol. Surv.* 1557 (1997).
7. Dorn, R. I. *et al.* Glacial chronology. *Res. Explor.* **7,** 456–471 (1991).
8. Gosse, J. C. & Phillips, F. M. Terrestrial *in situ* cosmogenic nuclides: theory and application. *Quat. Sci. Rev.* **20,** 1475–1560 (2001).
9. Trull, T. W. & Kurz, M. D. Experimental measurements of ^{3}He and ^{4}He mobility in olivine and clinopyroxene at magmatic temperatures. *Geochim. Cosmochim. Acta* **57,** 1313–1324 (1993).
10. Blard, P.-H. *et al.* Cosmogenic ^{3}He production rates revisited from evidences of grain size dependent release of matrix sited helium. *Earth Planet. Sci. Lett.* **247,** 222–234 (2006).
11. Reimer, P. J. *et al.* IntCal04 terrestrial radiocarbon age calibration, 0–26 cal kyr BP. *Radiocarbon* **46,** 1029–1058 (2004).
12. Peng, L. & King, J. W. A late quaternary geomagnetic secular variation record from Lake Waiau, Hawaii, and the question of the Pacific nondipole low. *J. Geophys. Res. Solid Earth* **97,** 4407–4424 (1992).
13. Schaefer, J. M. *et al.* Near-synchronous interhemispheric termination of the last glacial maximum in mid-latitudes. *Science* **312,** 1510–1513 (2006).
14. Vázquez-Selem, L. & Phillips, F. M. in *Program and Abstracts of the 15th Biennial Meeting, American Quaternary Association, AMQUA 1998, Northern Hemisphere-Southern Hemisphere Interconnections (5–7 September 1998; Puerto Vallarta, México)*, p. 174.
15. Smith, J. A., Seltzer, G. O., Farber, D. L., Rodbell, D. T. & Finkel, R. C. Early local last glacial maximum in the tropical Andes. *Science* **308,** 678–681 (2005).
16. Harper, J. T. & Humphrey, N. F. High altitude Himalayan climate inferred from glacial ice flux. *Geophys. Res. Lett.* **30,** 1764–1767 (2003).
17. Hock, R. A distributed temperature-index ice and snowmelt model including potential direct solar radiation. *J. Glaciol.* **45,** 101–111 (1999).
18. Porter, S. C. Pleistocene snowlines and glaciation of the Hawaiian Islands. *Quaternary Int.* **138,** 118–128 (2005).
19. Ludwig, K. R., Szabo, B. J., Moore, J. G. & Simmons, K. R. Crustal subsidence rate off Hawaii determined from $^{234}U/^{238}U$ ages of drowned coral reefs. *Geology* **19,** 171–174 (1991).
20. Hotchkiss, S. & Juvik, J. O. A. Late-Quaternary pollen record from Ka'au crater, O'ahu, Hawai'i. *Quat. Res.* **52,** 115–128 (1999).
21. Hostetler, S. W. & Clark, P. U. Tropical climate at the last glacial maximum inferred from glacier mass-balance modeling. *Science* **290,** 1747–1750 (2000).
22. Sicart, J.-E., Wagnon, P. & Ribstein, P. Atmospheric controls of the heat balance of Zongo Glacier (16°S, Bolivia). *J. Geophys. Res. Atmos.* **110,** doi:10.1029/2004JD005732 (2005).
23. Francou, B., Vuille, M., Wagnon, P., Mendoza, J. & Sicart, J. E. Tropical climate change recorded by a glacier in the central Andes during the last decades of the twentieth century: Chacaltaya, Bolivia, 16°S. *J. Geophys. Res. Atmos.* **108,** doi:10.1029/2002JD002959 (2003).
24. Hock, R. Temperature index melt modelling in mountain areas. *J. Hydrol.* **282,** 104–115 (2003).
25. Kitoh, A., Murakami, S. & Koide, H. A simulation of the last glacial maximum with a coupled atmosphere–ocean GCM. *Geophys. Res. Lett.* **28,** 2221–2224 (2001).
26. Lee, K. E. & Slowey, N. C. Cool surface waters of the subtropical North Pacific Ocean during the last glacial. *Nature* **397,** 512–514 (1999).
27. Hill, T. M. *et al.* Pre-Bølling warming in Santa Barbara Basin, California: surface and intermediate water records of early deglacial warmth. *Quat. Sci. Rev.* **25,** 2835–2845 (2006).
28. Kiefer, T. & Kienast, M. Patterns of deglacial worming in the Pacific Ocean: a review with emphasis on the time interval of Heinrich event 1. *Quat. Sci. Rev.* **24,** 1063–1081 (2005).
29. Johnsen, S. J., Dansgaard, W., Clausen, H. B. & Langway, C. C. Jr. Oxygen isotope profiles through the Antarctic and Greenland ice sheets. *Nature* **235,** 429–434 (1972).
30. Mikolajewicz, U., Crowley, T. J., Schiller, A. & Voss, R. Modelling teleconnections between the North Atlantic and North Pacific during the Younger Dryas. *Nature* **387,** 384–387 (1997).

Supplementary Information is linked to the online version of the paper at www.nature.com/nature.

Acknowledgements We thank E. Bard and S. Kidder for advice on the manuscript; S. Rowland and F. Trusdell for their assistance in the field; N. Humphrey for sharing his ice-flux Matlab code; G. Leduc, C. Vincent, R. Hock, D. Paillard, N. Thouveny, S. Sépulcre and G. Brocard for discussions that helped to improve glacial modelling and palaeoclimatic interpretations; and L. Zimmerman and B. Tibari for their analytical assistance in the Centre de Recherches Pétrographiques et Géochimiques (CRPG) noble gases laboratory. We thank the State of Hawaii for delivering sampling permits. Financial support was provided by the French INSU programme 'Relief de la Terre'.

Author Contributions P.-H.B. and J.L. conducted the field work in Hawaii, numerical modelling, data interpretation and paper writing. P.-H.B. and R.P. performed the cosmogenic ^{3}He analyses at CRPG (Nancy). P.W. provided ablation and climatic data from the Zongo glacier and helped in developing the glacier mass-balance model. D.B. participated in interpreting the cosmogenic data.

Author Information Reprints and permissions information is available at www.nature.com/reprints. The authors declare no competing financial interests. Correspondence and requests for materials should be addressed to P.-H.B. (blard@gps.caltech.edu or phb26@yahoo.fr).

METHODS

Determination of cosmogenic ^{3}He ages. ^{3}He cosmogenic concentrations (Supplementary Table 1) were converted into exposure ages, using a sea-level high-latitude production rate of 128 ± 5 atoms g^{-1} yr^{-1}. This empirical value was obtained from olivines with similar compositions to those analysed here[10]. The use of the same reference rate for pyroxenes is justified because ^3He_c concentrations are undistinguishable, within uncertainties, for both phenocrysts species coexisting within the same objects (MK9D and MK11, Supplementary Table 1). Ages were corrected for mask topography (less than 3%)[31] and boulder geometry (correction between 5% and 7%)[32]. Spatial and air-pressure corrections were performed by using the scaling factors of Stone[33], assuming that the island has been affected by a constant subsidence rate of 2.6 ± 0.4 mm kyr^{-1} (ref. 19). Effects of geomagnetic fluctuations on production rates were taken into account by using the corrections of Dunai[34] and the magnetic database of Carcaillet *et al.*[35]. These magnetic corrections are 6% and 3% for M2 and M0, respectively.

Glacier modelling. The cellular automata developed in ref. 16 was used to model the stationary state of the past glacial extents in Mauna Kea (details are given in Supplementary Information). This code was implemented with the mass-balance model described below.

'PDD-solar radiation' mass-balance model. The glacier mass balance was determined using an improved PDD model. This model, which integrates not only the pure temperature forcing but also the effect of solar radiation, has demonstrated its ability in reproducing the observed mass balance at high spatial and time resolutions[17]. Because the purpose of this study is to interpret the palaeoglacier in terms of mean palaeoclimatic variables, the mass balance was calculated over a one-year cycle, as follows.

The annual snow accumulation S (mm yr^{-1}) is the sum of the monthly snowfalls:

$$S = \sum_{i=1}^{12} S_i \tag{1}$$

S_i (mm per month) is calculated for each month assuming that precipitation falls as snow when the temperature is below the rain–snow threshold T_S. The PDD model assumes that temperatures have a normal distribution around the monthly mean temperature T_{mi}, with a standard deviation σ_i:

$$S_i = P_i \frac{1}{\sigma_i \sqrt{2\pi}} \int_{-\infty}^{T_S} e^{\frac{-(T-T_{mi})^2}{2\sigma_i^2}} dT \tag{2}$$

where P_i (mm per month) is the monthly precipitation. We assumed that T_S is 1 °C, which is a value reported from the tropical Andes[36]. Data do indeed show that below 0 °C 100% of precipitation is snow, and that above 2 °C 100% is rainfall. Moreover, weather stations of the Mauna Kea summit indicate that annual snowfalls are 125 ± 25 mm water equivalent, which is consistent with the value of 120 mm yr^{-1} predicted by our model and thus justifies the use of 1 °C for T_S. However, for Hawaii this parameter has a very limited influence on the climatic conclusions because Mauna Kea precipitations are particularly low (~250 mm yr^{-1} at 4,200 m). Indeed, a variation of ± 2 °C in T_S would induce an ELA shift of less than 50 m.

To consider the influence of albedo, which implies that the melting rate of ice is higher than that of snow (ice being darker than snow), we used different ablation parameters for snow and ice. The monthly ablation A_i (mm yr^{-1}) was calculated by assuming that the total melting is the sum of snow ablation A_{snow} and ice ablation A_{ice} (when ablation is sufficient to start melting the ice):

$$A_i = A_{snow}\,(i) + A_{ice}\,(i) \tag{3}$$

Given that α is the fraction of time during which ablation affects only snow, $\alpha = \frac{A_{snow}(i)}{A_i}$, we can write

$$A_{snow}(i) = \alpha \frac{365}{12} (M_{snow} + a_{snow} I_i) T_{Mi} \tag{4}$$

$$A_{ice}(i) = (1-\alpha) \frac{365}{12} (M_{ice} + a_{ice} I_i) T_{Mi} \tag{5}$$

where M_{snow} and M_{ice} (mm d^{-1} °C^{-1}) are the melt factors of snow and ice, respectively, a_{snow} and a_{ice} (mm d^{-1} W^{-1} m^2 °C^{-1}) are the radiation melt factors of snow and ice, respectively, I_i (W m^{-2}) is the mean monthly solar radiation, and T_{Mi} (°C) is the integrated monthly positive temperature.

Because, for each month, the amount of total snow input is known (S_i), equation (4) can be used to calculate α:

$$\alpha = \frac{\frac{12}{365} S_i}{(M_{snow} + a_{snow} I_i) T_{Mi}} \tag{6}$$

If $\alpha < 1$, the monthly total ablation A_i is not only sufficient to remove all the snow cover but it also starts melting the glacier ice. Then, in this case, A_i is calculated as

$$A_i = S_i + (1-\alpha) \frac{365}{12} (M_{ice} + a_{ice} I_i) T_{Mi} \tag{7}$$

In contrast, if $\alpha > 1$, the snow accumulation is higher than the total ablation; in this case, only snow melting occurs and monthly ablation A_i is

$$A_{snow}(i) = \frac{365}{12} (M_{snow} + a_{snow} I_i) T_{Mi} \tag{8}$$

Then the annual ablation A (mm yr^{-1}) is obtained by summing the monthly ablations:

$$A = \sum_{i=1}^{12} A_i \tag{9}$$

Past values of the solar radiation I_i are integrated over the appropriate period (19–16 kyr BP and 15 kyr BP for Hawaii) by using the astronomical corrections of ref. 37 and the numerical solution of ref. 38. At each grid cell, I_i is also corrected for the landscape characteristics, with

$$I_i = I_0 \left(\frac{R_m}{R_i}\right)^2 \psi^{\left(\frac{P}{P_0 \cos Zi}\right)} \cos\theta \tag{10}$$

where I_0 is the solar constant (1,368 W m^{-2}), R_i is the mean monthly Sun–Earth distance, R_m the mean Sun–Earth distance, $\psi = 0.75$ is the atmospheric clear-sky transmissivity, P and P_0 are the local and sea-level atmospheric pressure, respectively, Z_i is the mean monthly zenith angle and θ is the angle of incidence between the normal to the grid slope and the solar beams. For Hawaii, P and P_0 are from the daily radiosonde data of the Hilo International Airport over the period 1998–2002 (ref. 39).

The integrated monthly positive temperature T_{Mi} is computed with the PDD approach[40], which assumes that temperatures have a normal distribution around the monthly mean temperature T_{mi}, σ_i being the monthly standard deviation:

$$T_{Mi} = \frac{1}{\sigma_i \sqrt{2\pi}} \int_0^{\infty} T e^{\frac{-(T-T_{mi})^2}{2\sigma_i^2}} dT \tag{11}$$

Annual accumulation S and ablation A are calculated at each elevation by using equations (1) to (11). Finally, the mass balance elevation law, B_m (mm yr^{-1}) is computed by subtracting ablation from accumulation:

$$B_m = S - A \tag{12}$$

Calibration of the model parameters. Several studies[17,41] have reported empirical values for the parameters M and a, but these studies were conducted on Scandinavian glaciers. Therefore, to avoid any bias due to the tropical and high mountain specificities of Hawaii, we used the monitored mass balance data from a well-studied tropical glacier (Zongo, Bolivia, 16° S) to tune the parameters M_{snow}, M_{ice}, a_{snow} and a_{ice} (Supplementary Fig. 2).

The best fit yielded the following values:

$$M_{snow} = 3.7 \text{ mm d}^{-1} \text{ °C}^{-1}$$

$$M_{ice} = 7.4 \text{ mm d}^{-1} \text{ °C}^{-1}$$

$$a_{snow} = 2.8 \times 10^{-3} \text{ mm d}^{-1} \text{ W}^{-1} \text{ m}^2 \text{ °C}^{-1}$$

$$a_{ice} = 5.3 \times 10^{-3} \text{ mm d}^{-1} \text{ W}^{-1} \text{ m}^2 \text{ °C}^{-1}$$

These parameters are not significantly different from the empirical values determined in ref. 41. Moreover, the snow parameters are lower than those of ice, which suggests that this empirical model properly integrates the effects of albedo. After this preliminary calibration, the model was applied to the Mauna Kea volcano (19° N) with the climatic data recorded by the Hawaiian weather stations (Supplementary Figs 3–5).

31. Dunne, J., Elmore, D. & Muzikar, P. Scaling factors for the rates of production of cosmogenic nuclides for geometric shielding and attenuation at depth on sloped surfaces. *Geomorphology* **27,** 3–11 (1999).
32. Masarik, J. & Wieler, R. Production rates of cosmogenic nuclides in boulders. *Earth Planet. Sci. Lett.* **216,** 201–208 (2003).
33. Stone, J. O. Air pressure and cosmogenic isotope production. *J. Geophys. Res. Solid Earth* **105,** 23753–23759 (2000).
34. Dunai, T. J. Influence of secular variation of the geomagnetic field on production rates of *in situ* produced cosmogenic nuclides. *Earth Planet. Sci. Lett.* **193,** 197–212 (2001).
35. Carcaillet, J. T., Bourles, D. L. & Thouveny, N. Geomagnetic dipole moment and ^{10}Be production rate intercalibration from authigenic ^{10}Be/^{9}Be for the last 1.3 Ma. *Geochem. Geophys. Geosyst.* **5,** doi:10.1029/2003GC000641 (2004).
36. Lejeune, Y. *et al.* Melting of snow cover in a tropical mountain environment: processes and melting. *J. Hydrometeorol.* (in the press).
37. Laskar, J. *et al.* A long-term numerical solution for the insolation quantities of the Earth. *Astron. Astrophys.* **428,** 261–285 (2004).
38. Paillard, D., Labeyrie, L. & Yiou, F. Macintosh program performs time-series analysis. *Eos* **77,** 379 (1996).
39. NOAA. *Radiosonde Database Access* ⟨http://raob.fsl.noaa.gov/⟩ (2007).
40. Johannesson, T., Sigurdsson, O., Laumann, T. & Kennett, M. Degree-day glacier mass-balance modeling with applications to glaciers in Iceland, Norway And Greenland. *J. Glaciol.* **41,** 345–358 (1995).
41. Schuler, T. V. *et al.* Distributed mass-balance and climate sensitivity modelling of Engabreen, Norway. *Ann. Glaciol.* **42,** 395–401 (2005).